THE JOURNAL OF PHYSICAL CHEMISTRY B LETTERS

2005, *109,* 11858−11861
Published on Web 05/27/2005

Scattered Light Interference from a Single Metal Nanoparticle and Its Mirror Image

Sang-Kee Eah,[†,‡] Heinrich M. Jaeger,[†,§] Norbert F. Scherer,[†,||] Gary P. Wiederrecht,[⊥] and Xiao-Min Lin*[,‡,⊥]

Department of Physics and Department of Chemistry and The James Franck Institute, University of Chicago, Chicago, Illinois 60637, and Chemistry Division and Materials Science Division and Center for Nanoscale Materials, Argonne National Laboratory, Argonne, Illinois 60439

Received: March 4, 2005; In Final Form: April 29, 2005

The spatial distribution of surface plasmon scattering from a single nanoparticle changes dramatically near a metal surface as a result of interference from the direct scattered light and indirect scattered light from the mirror reflection. The unique interference patterns have been reproduced by simulations based on Huygens−Fresnel wave propagation theory. The large spectral width of the surface plasmon scattering enables a vertical distance measurement with 10 nm resolution through this nonintrusive far field interferometry.

Spontaneous light emission from many quantum systems is caused by single electron transitions between discrete energy levels. Changing the photonic mode density near a light emitter by placing it near a mirror or inside a cavity modifies the spatial distribution, decay rate, and resonance frequency of the light emission.[1] Experimentally, such effects have been observed in an ensemble of molecules deposited on a metal surface,[2] atoms traversing between two mirrors,[3−5] a single trapped electron,[6] and a single semiconducting quantum dot in an optical cavity.[7] These modifications are the essence of cavity quantum electrodynamics (QED) and have thus attracted considerable interest during the past several decades.

Light emission can also be generated by scattering from a small particle, a quasi-elastic process that originates from the collective oscillation of free electrons inside the particle. For gold (Au) or silver (Ag) nanoparticles, this collective oscillation generates a plasmon resonance in the visible region with a Lorentzian line shape.[8] Electromagnetic field enhancement induced by the surface plasmon and the chemical enhancement caused by molecular surface interaction are responsible for the enhanced Raman signals of molecules near (or at) the nanoparticle surface.[9,10] Coherent surface plasmon propagation along coupled nanoparticles has been proposed as an efficient way to transport energy on a small length scale.[11] Small metal nanoparticles are also being considered as alternative optical markers for biological applications, which can overcome the photobleaching and blinking problems facing the traditional organic dye molecules and semiconductor quantum dots.[12,13] It is therefore crucial to understand the effect of the local environment on surface plasmons. So far, most existing experiments have focused on the resonance frequency shift as a result of nearby dielectric or metallic media.[14−18] The spatial redistribution of scattered light in the presence of another interface or scatterer, especially on the single particle level, has not been thoroughly investigated. The main obstacles are the short dephasing time of the surface plasmon(<10 fs)[19,20] and the technical difficulty to manipulate a single nanoparticle. Understanding these effects, however, could have a much more significant implication in the area of nanoscale photonics.

In this letter, we demonstrate that, by adopting a novel dark field imaging technique, a unique interference pattern, in both spatial and spectral domains, can be obtained between the direct scattered light from a single Au nanoparticle and the indirect scattered light from its mirror image. The large line width of the surface plasmon enables us to determine the absolute vertical distance between the particle and the nearby metal surface with 10 nm resolution. Using this scheme, the ability to observe the interference effect is not limited by the dephasing time of the surface plasmon but instead limited by the spectral resolution of the spectrometer and the degree of defocusing of the reflected light on the detector. Theoretical simulations based on scalar wave diffraction theory reproduce all the features of the experiments. This shows that the light scattered by a single nanoparticle into different directions is spatially coherent.

Au nanoparticles with an average diameter of 80 nm were synthesized in an aqueous solution by sodium citrate reduction of Au salt. They were subsequently deposited on the surface of a 1 mm thick microslide glass at a sufficiently low density, so that the average interparticle distance is more than 20 μm. This allows isolated nanoparticles to be studied individually by the far field optical techniques without the interference of the nearby particles. Unlike traditional dark field imaging techniques,[19] we adopted a new scheme that frees up the space both below and above the sample. This allows simultaneous sample manipulation by an atomic force microscope (AFM) and optical detection in the far field with a large solid angle.[17] Figure 1 shows a schematic diagram of the experimental setup. White light from a halogen lamp is coupled into a multimode optical fiber with a 105 μm core diameter and directed to the side of the microscope slide. The evanescent wave created by the total

* Corresponding author. E-mail: xmlin@anl.gov.
[†] The James Franck Institute, University of Chicago.
[‡] Materials Science Division, Argonne National Laboratory.
[§] Department of Physics, University of Chicago.
[||] Department of Chemistry, University of Chicago.
[⊥] Chemistry Division and Center for Nanoscale Materials, Argonne National Laboratory.

10.1021/jp0511395 CCC: $30.25

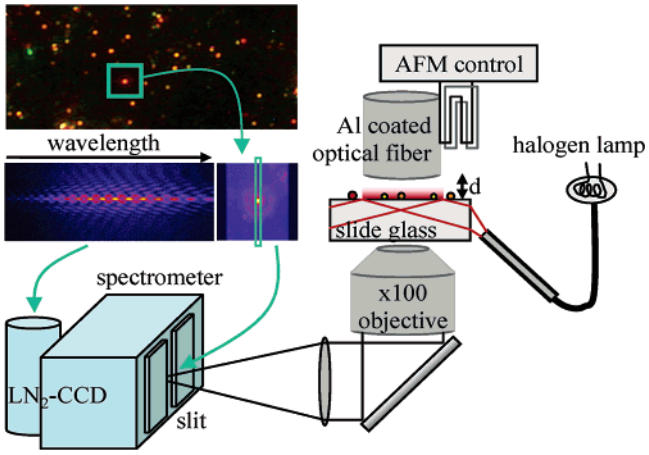

Figure 1. Schematic diagram of the experimental setup. White light from a halogen lamp is fed through a multimode optical fiber and coupled into a thin glass slide. Scattered light from a gold nanoparticle is collected by the objective lens and fed through a narrow entrance slit into a spectrometer which is coupled with a LN-CCD. A cleaved optical fiber coated with aluminum is controlled by an AFM and used as a micron size mirror.

internal reflection at the glass−air interface excites the nanoparticle. Only the scattered light from the Au nanoparticle propagates to the far field, and it is collected by a long working distance (6 mm) 100× magnification objective lens (Mitutoyo) with a numerical aperture (NA) of 0.7 and an effective focal length of 2 mm. A 100 μm entrance slit was used to select a narrow strip of the interference pattern in real space (*y*-direction in Figure 2) and dispersed with the imaging spectrometer (Jobin Yvon Triax-190) into different wavelengths (*x*-direction in Figure 2). The optical signal was collected by a two-dimensional liquid nitrogen cooled charge-coupled device (LN-CCD) camera (Jobin Yvon) with an integration time of 10 s. A single mode optical fiber was cleaved, and its flat end surface was coated with a thin film of aluminum to form a flat mirror with a diameter of 125 μm. With a tuning fork attached, the distance between the mirror surface and glass surface can be controlled by an AFM controller (Omicron).

Without the mirror, the surface plasmon scattering from a single relatively spherical Au nanoparticle has a Lorentzian line shape, whereas a nonspherical particle or an aggregate of particles typically has a nonsymmetric line shape. This trend was verified by combining optical spectroscopy measurements with scanning electron microscopy on the same sample and used as a criterion for selecting an isolated spherical nanoparticle for the experiments. Nonspherical particles can also be resolved from the asymmetrical spatial distribution of scattered light, which can be obtained by slightly defocusing the image at the detector and allowing the signal to be collected on a larger area on the detector.[21] Figure 2a shows the scattering spectrum from a particle that has a spectral width of 68 THz, which corresponds to a dephasing time of 2.4 fs. We did not control the excitation light polarization using the multimode optical fiber. However, due to the spatial distribution of the dipole field and the experimental setup, the majority of the scattered light collected by the objective lens comes from the dipole oscillation that is parallel to the glass surface.

A unique interference pattern develops along both the spectral axis (*x*-direction) and the spatial axis (*y*-direction) when the

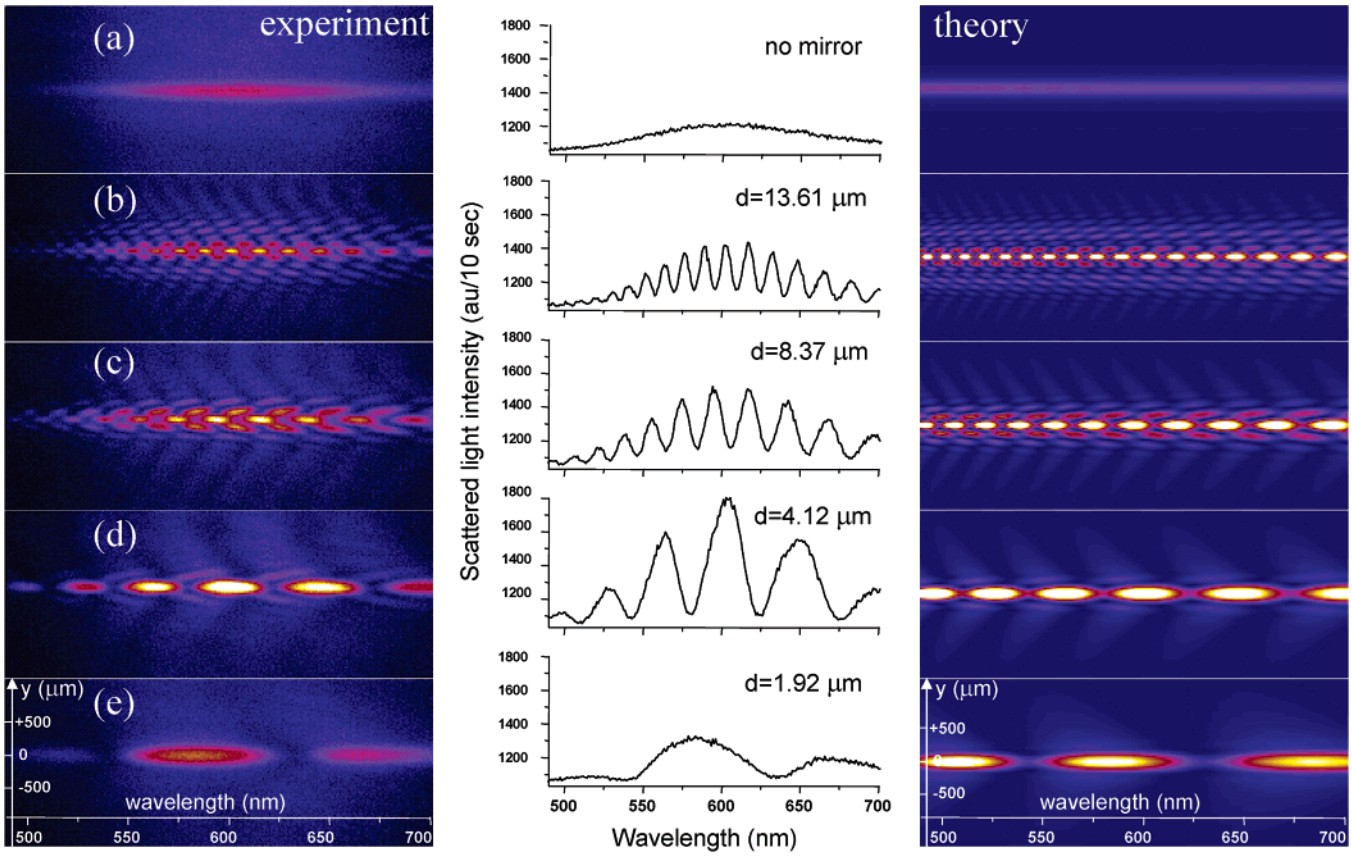

Figure 2. Plasmon scattering light interference patterns of a single gold nanoparticle near a metal mirror with various spacings. The *y*-axis represents the vertical slice of the spatial light distribution, which is dispersed into different wavelengths along the *x*-axis. The experimental results are shown in the left column. The intensity variation along the wavelength at $y = 0$ is shown in the center column, and that corresponding to theoretical simulation results is shown in the right column.

mirror approaches the surface. The left column of Figure 2 shows the experimental data at several different mirror−particle distances. Surprisingly, even with the mirror−particle separation at 2 orders of magnitude larger than the wavelength of the light, the interference pattern is clearly visible. This interference phenomenon can be understood as the superposition of the light scattered directly from the nanoparticle and the scattered light reflected from the mirror. The light intensity at the center of the detector ($y = 0$) oscillates with wavelength (central column in Figure 2). The period becomes longer as we decrease the mirror−particle distance or increase the wavelength. No visible interference pattern is observed when the CCD integration time is set at 0.1 s, because of the insufficient signal accumulation of the discrete single photon events. Long integration times (10 s in Figure 2) or superposing many images taken for short integration time yields the interference patterns.

To reproduce the complex interference pattern by numerical simulation, especially the Y-shaped features near $y = 0$ in Figure 2b−d, we consider the propagation of both the direct scattered light and the indirect scattered light through the lens system. In our simulation, the direct scattered light was approximated using the field created by a dipole that is parallel to the glass surface. It ultimately focuses on the detector (Figure 3a). The reflected light from the mirror is approximated by an image dipole that is defocused on the detector. Different in-plane orientations of the dipole were averaged to match the condition of our experiment. The propagation of the light through the lens system with a finite numerical aperture is calculated using the scalar wave diffraction theory based on the Huygens−Fresnel principle.[22] For instance, the complex field amplitude, $U(\vec{r}')$, at the detector is a superposition of spherical waves from oscillators on the spherical plane of the tube lens

$$U(\vec{r}') = \frac{f^2}{i\lambda}\int\int d\Omega (U_r(\vec{r}) + U_i(\vec{r}))\frac{e^{(i(2\pi/\lambda)s)}}{s} \qquad (1)$$

where f is the focal length of the tube lens, $U_r(\vec{r})$ and $U_i(\vec{r})$ are complex field amplitudes at the tube lens induced by the real dipole and the image dipole, respectively, and $s = |\vec{r}' - \vec{r}|$ is the distance between the tube lens integration point and the detector position. The integration solid angle is determined by the numerical aperture of the tube lens. In a similar fashion, the complex fields on the tube lens, $U_r(\vec{r})$ and $U_i(\vec{r})$, were calculated from the field distribution on the spherical plane of the objective lens. The radii of the integration surfaces are the focal lengths of the objective lens (2 mm) and tube lens (248 mm), respectively, and are determined by their magnification. The extra path lengths caused by the 1 mm thick microscope slide glass were also taken in account.

The simulation results are shown in the right column of Figure 2. They reproduce all the major features observed in the experiment. The spectral envelope of the surface plasmon was not included in the simulation in order to make the spectral features more visible. Interference between the light from the real dipole and the image dipole causes a redistribution of light in space. Such a modification can be clearly seen in Figure 3b, which shows the light intensity distribution on a cross-sectional plane after the objective lens. A more straightforward revelation of how the interference pattern is generated is shown in Figure 3c and d, where the intensity distributions from the real and image dipoles on the detector are shown separately before being superimposed. The real dipole field has a tight focus spot on the detector, and its size has a slight wavelength dependence. On the other hand, the image dipole is defocused, with several self-interference rings. This field distribution from a defocused

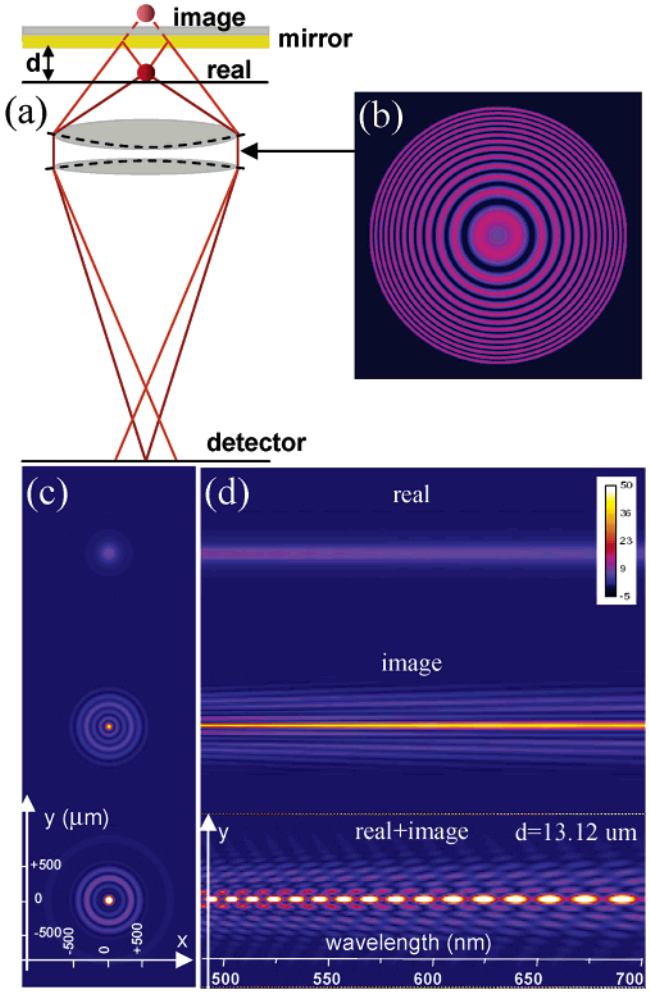

Figure 3. (a−c) Theoretical simulation results of the interference at the mirror distance $d = 13.12$ μm and wavelength $\lambda = 600$ nm. (a) Schematic diagram showing the objective lens is focused to the real dipole of the single gold nanoparticle and the image dipole created by the metal surface is defocused at the detector. (b) The interference between the two dipoles generates concentric rings at a plane after the objective lens. (c and d) The spatial and spectral distribution of the real dipole only (top panels) and the image dipole only (middle panel) and superposition of the real and image dipole fields (bottom panel).

dipole was independently verified experimentally by removing the mirror and defocusing the image on the detector. The interference pattern extends far away from the center, even though the light intensity from the real dipole is relatively small in this area. The high visibility of the interference is caused by the relative phase shift between the two dipole fields.

Because of the short dephasing time of the surface plasmon, scattering from a metal nanoparticle typically has a large spectral width. This creates the complex interference pattern observed in the experiments. By analyzing this pattern, we can determine the distance between the nanoparticle and the mirror surface. If we consider only the light travelling along the optical axis, the relative phase shift between the two consecutive destructive interference wavelengths (λ_1 and λ_2) is 2π. The absolute distance (d) between the nanoparticle and the mirror can be estimated by $d = (1/2)\lambda_1\lambda_2/(|\lambda_1 - \lambda_2|)$. To determine the distance more precisely, we need to take into account all the light collected by the objective lens in a numerical simulation and compare the results with the experimental data. Figure 4 shows the intensity distribution at two particle−mirror distances for both the experiment and the simulation. It is clear that a resolution

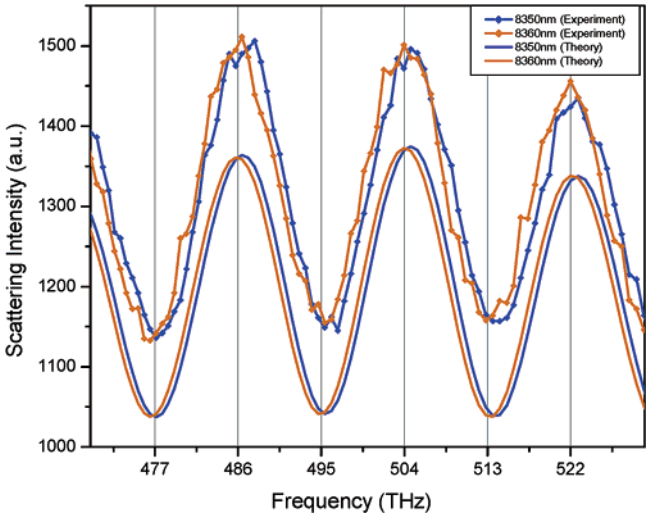

Figure 4. The particle−mirror distance can be determined with a spatial resolution of 10 nm based on the shift of interference patterns. The top two curves correspond to the experimental data at particle−mirror distances of 8350 and 8360 nm (at $y = 0$). The bottom two curves are the corresponding simulation results. (The data are vertically shifted for clarity.)

of 10 nm can be readily achieved in our experiment. By improving the stability of our optical system, it is anticipated that a resolution of a few nanometers can be achieved. The maximum distance that can be determined by this technique is limited by the spectral resolution of the spectrometer and the decrease of the visibility due to the defocusing of the image dipole. The smallest distance that can be determined (i.e., nanometer resolution) is limited by the spectral width of the plasmon. The accurate distance measurement depends on matching the destructive interference minima (or constructive maxima) with the simulation results. As the distance between the particle and mirror decreases, the number of interference minima within the envelope of the surface plasmon decreases quickly. When the number of minima within the envelope drops below two, it becomes very difficult to determine the absolute particle−mirror distance accurately. This sets the lower limit for distance measurements using a single particle. In our experiments, the range of distances that can be determined accurately extends from $d = 1.5$ μm to 33 μm.

There is great potential to use small nanocrystals as biological labels to study biological processes.[23] Metal nanocrystals have the advantage that the surface plasmon does not suffer from problems such as spectral diffusion and stochastic blinking which are typical for fluorescent emitters. The accurate determination of the position of the particle in three-dimensional space could yield important information about biological processes and their time evolution, such as motion of subcellular structure (e.g., actin fibers). The most important advantage of our single particle interference technique is that both the probe (reflecting mirror) and the detector can be placed far away from the sample (tens of microns) and still yield nanometer resolution in the vertical direction. Thus, it is a much less intrusive technique as compared with atomic force microscopy, which requires direct contact between the probe and the sample. Locating the particle in the lateral directions (x,y) can be achieved by fitting the scattering spatial profile with a Gaussian. The peak position of the Gaussian can be determined with nanometer resolution, similar to what has been done in single molecule fluorescence measurement.[24,25] A technical challenge in applying this interference technique to a real system does, however, arise from the need to locate the particle within the region of the evanescent wave at the glass−air interface. To mitigate this issue, it may be necessary to apply a different dark field illumination technique.

Acknowledgment. This work was supported by the University of Chicago−Argonne National Laboratory Consortium for Nanoscience Research. Additional support came from the NSF MRSEC program under Award No. DMR-0213745 (H.M.J. and N.F.S.). X.-M.L. acknowledges support from the U.S. Department of Energy, Basic Energy Sciences-Materials Sciences, under Contract No. W-31-109-ENG-38.

Supporting Information Available: Movies of interference pattern evolution as the distance between the nanoparticle and the mirror is continuously changed. This material is available free of charge via the Internet at http://pubs.acs.org.

References and Notes

(1) Barnes, W. L. *J. Mod. Opt.* **1998**, *45*, 661.
(2) Drexhage, K. H. *Progress in Optics*; Wolf, E., Ed.; North-Holland: Amsterdam, The Netherlands, 1974.
(3) Jhe, W.; Anderson, A.; Hinds, E. A.; Meschede, D.; Moi, L.; Haroche, S. *Phys. Rev. Lett.* **1987**, *58*, 666.
(4) Heinzen, D. J.; Feld, M. S. *Phys. Rev. Lett.* **1987**, *59*, 2623.
(5) McKeever, J.; Boca, A.; Boozer, A. D.; Miller, R.; Buck, J. R.; Kuzmich, A.; Kimble, H. J. *Science* **2004**, *303*, 1992.
(6) Gabrielse, G.; Dehmelt, H. *Phys. Rev. Lett.* **1985**, *55*, 67.
(7) Pelton, M.; Santori, C.; Vuckovic, J.; Zhang, B.; Solomon, G. S.; Plant, J.; Yamamoto, Y. *Phys. Rev. Lett.* **2002**, *89*, 233602.
(8) Kreibig U.; Vollmer M. *Optical Properties of Metal Clusters*; Springer: Berlin, 1995.
(9) Schatz, G. C.; Van Duyne, R. P. *Handbook of Vibrational Spectroscopy*; Chalmers, J. M., Griffiths, P. R., Eds.; Wiley: New York, 2002.
(10) Campion, A.; Kambhampati, P. *Chem. Soc. Rev.* **1998**, *27*, 241.
(11) Quinten M.; Leitner, A.; Krenn, J. R.; Aussenegg, F. R. *Opt. Lett.* **1998**, *23*, 1331.
(12) Boyer, D.; Tamarat, P.; Maali, A.; Lounis, B.; Orrit, M. *Science* **2002**, *297*, 1160.
(13) Cognet, L.; Tardin, C.; Boyer, D.; Choquet, D.; Tamarat, P.; Lounis, B. *Proc. Natl. Acad. Sci. U.S.A.* **2003**, *100*, 11350.
(14) Mock, J. J.; Smith, D. R.; Schultz, S. *Nano Lett.* **2003**, *3*, 485.
(15) Raschke, G.; Kowarik, S.; Franzl, T.; Sönnichsen, C.; Klar, T. A.; Feldmann, J. *Nano Lett.* **2003**, *3*, 935.
(16) McFarland, A. D.; Van Duyne, R. P. *Nano Lett.* **2003**, *3*, 1057.
(17) Eah, S.-K.; Jaeger, H. M.; Scherer, N. F.; Wiederrecht, G. P.; Lin, X.-M. *Appl. Phys. Lett.* **2005**, *86*, 031902.
(18) Holland, W. R.; Hall, D. G. *Phys. Rev. Lett.* **1984**, *52*, 1041.
(19) Sönnichsen, C.; Franzl, T.; Wilk, T.; von Plessen, G.; Feldmann, J.; Wilson, O.; Mulvaney, P. *Phys. Rev. Lett.* **2002**, *88*, 077402.
(20) Liu, Y.-H.; Unterreiner, A. N.; Chang, Q.; Scherer, N. F. *J. Phys. Chem. B* **2001**, *105*, 2135.
(21) Bartko, A. P.; Dickson, R. M. *J. Phys. Chem. B* **1999**, *103*, 11237.
(22) Born M.; Wolf, E. *Principles of Optics: Electromagnetic Theory of Propagation, Interference and Diffraction of Light*; Cambridge University Press: Cambridge, U.K., 1999.
(23) Alivisatos, P. *Nature Biotechnol.* **2004**, *22*, 47.
(24) Yildiz, A.; Forkey, J. N.; Mckinney, S. A.; Ha, T.; Goldman, Y. E.; Selvin, P. R. *Science* **2003**, *300*, 2061.
(25) Qu, X.; Wu, D.; Mets, L.; Scherer, N. F. *Proc. Natl. Acad. Sci. U.S.A.* **2004**, *101*, 11298.